

Quantum-fluctuation-induced repulsive interaction of a quantum string between walls

Yoshihiro Nishiyama

Department of Physics, Faculty of Science, Okayama University, Okayama 700-8530, Japan

(Received 29 January 2001; revised manuscript received 9 April 2001; published 19 July 2001)

A quantum string, which was brought into discussion recently as a model for the stripe phase in doped cuprates, is simulated by means of the density-matrix-renormalization-group method. String collides with adjacent neighbors, as it wanders, owing to quantum zero-point fluctuations. The energy cost due to the collisions is our main concern. Embedding a quantum string between rigid walls with separation d , we found that for sufficiently large d , collision-induced energy cost obeys the formula $\sim \exp(-Ad^\alpha)$ with $\alpha=0.808(1)$, and the string's mean fluctuation width grows logarithmically $\sim \log d$. Those results are not understood in terms of a conventional picture that the string is "disordered," and only short-wavelength fluctuations contribute to collisions. Rather, our results support a recent proposal that owing to collisions, short-wavelength fluctuations are suppressed, but instead, long-wavelength fluctuations become significant. This mechanism would be responsible for stabilizing the stripe phase.

DOI: 10.1103/PhysRevB.64.064510

PACS number(s): 74.90.+n, 46.70.Hg, 05.10.-a, 05.30.-d

I. INTRODUCTION

Recently, Zaanen brought up a problem of "quantum string,"¹ which is a linelike object subjected to line tension, and it wanders owing to quantum-mechanical zero-point fluctuations. Central concern is to estimate the interaction between adjacent strings as it wanders quantum-mechanically and undergoes entropy-reducing "collisions" with their neighbors. Statistical mechanics of quantum-string gas would be relevant to the low-energy physics of the so-called stripe phase observed experimentally in doped cuprates.²⁻⁴ In particular, one is motivated to gain insights how the stripe pattern formed in cuprates acquires stability. Actually, a good deal of theoretical analyses had predicted tendency toward stripe-pattern formation.⁵⁻¹¹ However, first-principle simulations on the t - J model still remain controversial about that issue.¹²⁻¹⁴ The aim of the aforementioned recent analysis¹ is to shed light, particularly, on the role of the quantum fluctuations and the entropy-reducing collisions at the expense of disregarding microscopic constituents of quantum string.

In the path-integral space-time picture, quantum string spans a world sheet as time evolves.¹⁵ Hence, one may wonder that physics of quantum string might bear resemblance to that of membrane, and so quantum string is readily understood through resorting to the past outcomes about membrane.¹⁶⁻²² However, elasticities are different: Quantum-string's elastic energy is quadratic in its slope (line tension), whereas membrane's is quadratic in its curvature (bending elasticity). This seemingly slight difference causes, according to Ref. 1, distinctive behaviors.

When quantum string is laid down in a free space, its Hamiltonian is quadratic, and thus no peculiarity emerges. (We will introduce the Hamiltonian afterwards.) Yet, when it is squeezed by adjacent neighbors or walls, there immediately arise awful complications due to many-body correlations. In order to tackle with the string gas, Zaanen employed Helfrich's technique,^{23,24} that has been utilized in the course of the studies of stacked membranes. Thereby, he arrived at the conclusion that collision-induced energy cost f would be

described by $f \sim \exp(-Ad^{2/3})$ with string interval d . That result cannot be understood in terms of conventional argument²⁵ which gives $f \sim \exp(-Ad^2)$; this argument is based on such picture that string is "disordered," and the collisions are mainly due to short-wavelength meandering modes. (We will outline this argument in Sec. III B.) On the contrary, Zaanen emphasizes the role of long-wavelength fluctuations, because his theory is sensitive to infrared cutoff.

The purpose of this paper is to judge the validity of those scenarios by performing first-principle simulations. We put a quantum string between rigid walls with spacing d , and measured its repelling interaction by observing pressure against the walls. [This trick has been used in the studies of the fluctuation pressure of (classical) membrane.¹⁶⁻¹⁸] The Hamiltonian, which we had simulated, is given by

$$\mathcal{H} = \sum_{i=1}^L \left(\frac{p_i^2}{2m} + V(x_i) \right) + \sum_{i=1}^{L-1} \frac{\Sigma}{2} (x_i - x_{i+1})^2. \quad (1)$$

Here, x_i denotes the operator of transverse displacement of a particle at i th site, and p_i is its conjugate momentum. They satisfy the canonical commutation relations $[x_i, p_j] = i\hbar \delta_{ij}$, $[x_i, x_j] = 0$ and $[p_i, p_j] = 0$. $V(x)$ is rigid-wall potential with spacing d ,

$$V(x) = \begin{cases} 0 & \text{for } 0 \leq x \leq d, \\ \infty & \text{otherwise.} \end{cases} \quad (2)$$

Σ denotes line tension which puts particles into line. Classical version of this Hamiltonian has been used as a model for line dislocations and steps on (vicinal) surfaces.^{26,27} Note that for sufficiently large Σ , one can take continuum limit, with which one arrives at field-theoretical version of quantum string. Such continuum-limit version was studied analytically in Ref. 1.

The rest of this paper is organized as follows. In the next section, we explicate our simulation scheme. We used diagonalization method: Note that elastic models such as ours (1) have vast number of vibration modes, which overwhelm computer-memory size. Emphasis is laid upon the point how

we had adopted the idea of density-matrix renormalization group^{28,29} to quantum string so as to reduce the number of Hilbert-space bases. Our algorithm is indebted to recent developments,^{30–32} where a polaron model (lattice vibration) was simulated with use of the density-matrix renormalization group; see also Ref. 33. Following the preparations, in Sec. III, we perform numerical calculation. We show that our first-principle simulation supports aforementioned Zaanen's scenario. In the last section, we give summary and discussions.

II. DETAILS OF NUMERICAL METHOD: DENSITY-MATRIX RENORMALIZATION GROUP

In this section, we explain our simulation algorithm. As is mentioned below, our algorithm is based on recent proposals, where the idea of the density-matrix renormalization group^{28,29} is applied to the problem of phonon and polaron.^{30–32} We will also show preliminary simulation data so as to demonstrate reliability of our calculation.

Quantum string is made of many particles connected with line tension Σ . Each particle spans infinite-dimensional Hilbert space. Hence, one is forced to truncate, somehow, the number of bases in order to diagonalize the Hamiltonian. Even though one truncated bases of each particle, the total bases of quantum string, as a whole, would exceed available computer-memory size. This difficulty arises inevitably in

treating elastic (bosonic) degrees of freedom by means of diagonalization. Recently, however, it has been reported that the difficulty is overcome by an application of the density-matrix renormalization group.^{30–32} In the following, based on these developments, we present our simulation scheme; we tried to provide enough details for the reader who might want to implement it.

Our algorithm is recursive; after the completion of one recursion (renormalization), the number of treated particles (length of quantum string) is enlarged by two, and subsequent renormalization follows. In the following, we explain steps constituting one renormalization procedure: Suppose that our system (quantum string) is decomposed into four parts, that is, block, site, site and block, in this order. After one renormalization is completed, composite systems of block and site are “renormalized” into a new block with block Hilbert-space dimension *unchanged*.

As would be guessed, “site” merely stands for one particle of quantum string. We then need to prepare bases to represent the Hilbert space of “site.” We had chosen such M bases that are the eigenstates $|n\rangle_{\bullet}$ ($n=1\sim M$) of the intrasite Hamiltonian $\mathcal{H}_{\bullet}=p^2/(2m)+V(x)$ with energy $E_n=\hbar^2\pi^2n^2/(2md^2)$. (Therefore, the direct product of $|n\rangle_{\bullet}$ gives the eigenstate of the total Hamiltonian \mathcal{H} , provided that the line tension is tuned off ($\Sigma=0$.) With respect to these bases $\{|n\rangle_{\bullet}\}$ ($n=1\sim M$). We represent the matrix of the x_i operator,

$$[x_{\bullet}]_{nm} = \langle n|x|m\rangle_{\bullet} = \begin{cases} \frac{2d}{\pi^2} \left(\frac{1}{(m+n)^2} - \frac{1}{(m-n)^2} \right), & (n,m) = (\text{even,odd}) \text{ or } (\text{odd,even}), \\ 0, & \text{otherwise.} \end{cases} \quad (3)$$

The truncation bound M is one source of numerical errors. We need to choose M sufficiently large; we will demonstrate afterwards that this truncation does not deteriorate simulation precision in practice.

Let us turn to explaining “block.” The “block” stands for a part (fragment) of quantum string, and actually, it contains many particles in it. Hence, at a glance, one may wonder that the Hilbert-space dimension of block would be extremely large. Yet, owing to the density-matrix renormalization, the dimension is reduced so that it can be stored in computer memory. The Hilbert space of block is spanned by those bases $|n\rangle_{\text{B}}$ ($n=1\sim m$). The bases are to be prepared in the *preceding* renormalization procedure; see below. With respect to these bases, one has to represent the intrablock Hamiltonian \mathcal{H}_{B} and the coordinate operator of the particle at the end of “block” x_{B} ; see below. At the initial stage of renormalization, the block is merely a “site,” and so we start with $\mathcal{H}_{\text{B}}=\mathcal{H}_{\bullet}$, $x_{\text{B}}=x_{\bullet}$ and $m=M$.

Provided that the above matrices are at hand, the (total) Hamiltonian $\mathcal{H}(=\mathcal{H}_{\text{B}\bullet\text{B}})$ of quantum string is expressed in terms of them. Diagonalizing this matrix, one obtains the ground state,

$$|\psi\rangle = \sum_{ijkl} \psi_{ijkl} |i\rangle_{\text{B}} |j\rangle_{\bullet} |k\rangle_{\bullet} |l\rangle_{\text{B}}. \quad (4)$$

With use of ψ_{ijkl} , we obtain the density matrix for the left-half subsystem ($\text{B}+\bullet$);

$$[\rho]_{i,j;i',j'} = \sum_{kl} \psi_{ijkl} \psi_{i'j'kl}^*. \quad (5)$$

Diagonalizing this, we obtain the eigenstates and the eigenvectors; $\rho|u_n\rangle = w_n|u_n\rangle$ with $w_1 > w_2 > \dots > w_{(M \times m)}$. Those bases $|u_n\rangle$ with large weight w_n would be important (relevant) in order to describe the physics of the subsystem of block and site. Therefore, we store the bases $|u_n\rangle$ with $n=1\sim m$, and discard the others. This criterion is the essence of the so-called density-matrix renormalization group.^{28,29} That truncation may cause another source of numerical errors. Later, we will demonstrate that this error is very small. Finally, we perform the “density-matrix renormalization,”

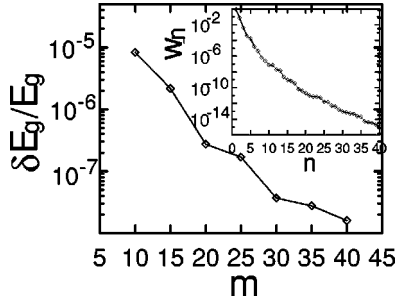


FIG. 1. Relative error of the ground-state energy for the system with $d=4$, $\Sigma=4$, $L=8$, and $M=9$. “Exact” energy is calculated with respect to the full Hilbert-space dimensions $M^L=9^8$, while “approximate” energy is calculated for truncated “block” bases m with use of the density-matrix renormalization group. Ground-state-energy difference between them gives δE_g . Note that the truncated-base calculation with small m reproduces the full-diagonalization result very precisely. Inset shows the density-matrix eigenvalues $\{w_n\}$, which are used for monitoring simulation precision; see text for details.

$$[\mathcal{H}_{B'}]_{nm} = \left\langle u_n \left| \mathcal{H}_B \otimes \hat{1} + \hat{1} \otimes \mathcal{H}_\bullet + \frac{\Sigma}{2} (x_B^2 \otimes \hat{1} - 2x_B \otimes x_\bullet + \hat{1} \otimes x_\bullet^2) \right| u_m \right\rangle, \quad (6)$$

$$[x_{B'}]_{nm} = \langle u_n | \hat{1} \otimes x_\bullet | u_m \rangle. \quad (7)$$

Now, a renormalization is completed. We can restart the next renormalization from the beginning, replacing the renormalized block B' with B . It is to be noted that through the renormalization, the block dimension is kept within m .

In the following, we will show that the above algorithm actually works. In Fig. 1, we plotted the relative error of the ground-state energy $\delta E_g/E_g$ for the system with $\Sigma=4$ and $d=4$. (This parameter condition is of great physical significance as would be shown in Sec. III.) The system size is $L=8$, and the dimension of “site” is $M=9$. Therefore, the full number of bases is $M^L=43046721$, which is about to exceed the limit of available computer-memory size and is barely manageable with full diagonalization method. For these full bases, we calculated the “exact” ground-state energy, while “approximate” energy is calculated by means of the density-matrix renormalization group with truncated “block” dimension m . The energy difference between them gives δE_g . The relative error $\delta E_g/E_g$ is plotted in Fig. 1. We achieve very small error 10^{-8} with $m=20$, for which the total number of bases is no more than $20^2 \cdot 8^2=25600$. Hence, we see that our algorithm works efficiently. The inset of Fig. 1 shows the distribution of the density-matrix eigenvalues $\{w_n\}$. Usually, w_n is utilized for monitoring $\delta E_g/E_g$, because they look alike. However, in our case, there are discrepancies in their magnitudes. The discrepancies may be due to the fact that our Hamiltonian matrix elements distribute over wide range. By the way, we chose m corresponding to $w_m=10^{-12}$ in Sec. III. In this way, we kept precision within 10^{-7} . Typically, we need, at most, $m=30$ bases.

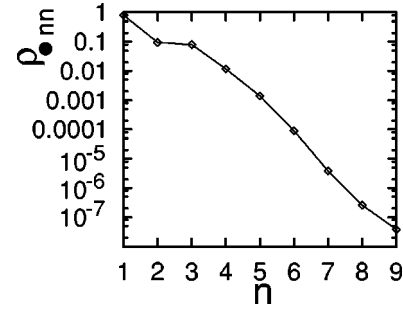


FIG. 2. Probability weight $[\rho_\bullet]_{nn}$ of the state $|n\rangle_\bullet$ is plotted. This plot indicates how site-dimension truncation M affects the reliability of simulation. Probability weight for $n=9$ is negligibly small; $[\rho_\bullet]_{99} \approx 10^{-7}$. Hence, truncation of those states with $n>9$ does not deteriorate any reliability in practice. In Sec. III, we impose an even severer request $[\rho_\bullet]_{MM} \approx 10^{-10}$.

In the above, we have checked that the truncation of block dimension m does not harm any reliability of our simulation. Finally, we will examine the influence of site-dimension truncation M . In order to see that, it is sensible to monitor

$$[\rho_\bullet]_{jj'} = \sum_{ikl} \psi_{ijkl} \psi_{ij'kl}^*. \quad (8)$$

As would be apparent from the definition, $[\rho_\bullet]_{nn}$ tells the degree of significance of the state $|n\rangle_\bullet$. Because we use the bases of $n=1-M$ and discard the others, it should be checked whether $[\rho_\bullet]_{MM}$ is small enough. We see from Fig. 2 that the $M=9$ state is of very rare probability 10^{-7} . In the subsequent simulations in Sec. III, we impose even severer request $[\rho_\bullet]_{MM} = 10^{-10}$. In order to match this request, we need, at most, $M=20$ bases; hence, the maximal total number of Hilbert-space bases is no more than $m^2 \cdot M^2 = 30^2 \cdot 20^2 = 360000$. As is mentioned above, the full diagonalization of Figs. 1 and 2 requires the Hilbert-space dimensions 43046721 for string length $L=8$. It is far beyond the capability of the diagonalization method to treat longer string, unless we resort to the density-matrix renormalization group.

Finally, let us mention the choice of the local basis for the local degree of freedom; we used low-lying eigenstates $|n\rangle_\bullet$ for the rigid-wall potential. One may wonder that another choice, for instance, a set of local oscillator eigenstates, would be more efficient, because it would capture the string’s vibration adequately. However, this idea does not work, because it does not match the boundary condition that the wave function should vanish at rigid walls. In other words, existence of the rigid walls is taken into account in our formalism through the boundary condition.

III. NUMERICAL RESULTS AND DISCUSSIONS

In this section, we present simulation results. In our simulation, we treated sufficiently large system sizes by repeating renormalizations, until the simulation result converges to a (thermodynamic) limit. System parameters of m and \hbar are fixed; namely, we set $m=1$ and $\hbar=1$. those parameters just fix the coefficient of the kinetic-energy term. Therefore, the choice of parameters does not harm any generality. Technical

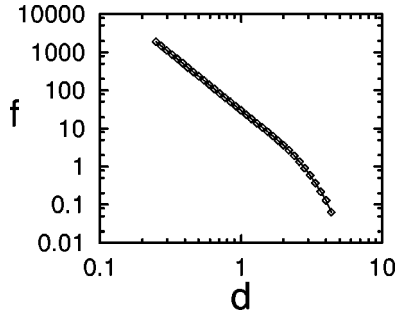


FIG. 3. Excess energy cost due to collisions f (9) is plotted for $\Sigma=4$ and various d . We see that for $d<2$, it obeys power law $f \sim d^{-3}$, while for $d>2$, it drops rapidly.

details are to be referred to the previous section.

A. Collision-induced energy cost f and elasticity modulus B

In Fig. 3, we plotted the collision-induced energy cost,

$$f = \frac{E_g(d) - E_g(d \rightarrow \infty)}{d}, \quad (9)$$

for the system with line tension $\Sigma=4$ and various wall spacing d . Here, $E_g(d)$ denotes the ground-state energy per one particle for wall spacing d . As would be apparent from the definition (9), f measures excess energy cost (per unit volume) due to the presence of walls. It is notable that $E_g(d \rightarrow \infty)$ is calculated exactly,

$$E_g(d \rightarrow \infty) = \frac{1}{2\pi} \int_{-\pi}^{\pi} dk \sqrt{\frac{\Sigma}{m}} \left| \sin \frac{k}{2} \right|, \quad (10)$$

because for $d \rightarrow \infty$, the Hamiltonian reduces to quadratic form.

In Fig. 3, we notice that two distinctive regimes exist: For $d < 2$, the collision energy f decreases obeying power law,

$$f \sim 1/d^3, \quad (11)$$

whereas for $d > 2$, it decays ‘‘rapidly,’’ actually, it is our main concern to clarify how ‘‘rapid’’ it decays. The behavior for $d < 2$ is understood immediately: Suppose that the line tension is turned off ($\Sigma=0$), each particle becomes independent, and it reduces to a text-book problem of ‘‘particle in a box,’’ for which the ground-state energy is solved exactly; $E_g = \hbar^2 \pi^2 / (2md^2)$. Hence, we arrive at the relation $f = E_g/d \sim 1/d^3$. To summarize, for small $d < 2$, inter-particle interaction is irrelevant. On the other hand, for large d , the interparticle interaction may become relevant. Because of this, the particles become correlated, and f drops very rapidly.

In order to elucidate characteristics of fluctuation-induced interaction, it is sensible to calculate the elasticity modulus which is defined by the formula

$$B = d^2 \frac{\partial^2 f}{\partial d^2}. \quad (12)$$

In Fig. 4, we plotted B for the same parameter range as that

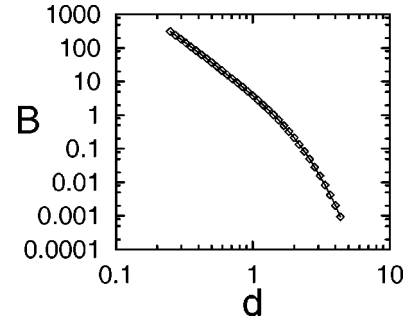


FIG. 4. Elasticity modulus B (12) is plotted for the same parameter range as that of Fig. 3. We see that for $d<2$, it obeys power law $B \sim d^{-3}$, while for $d>2$, B drops rapidly.

of Fig. 3. As well as f , B also exhibits two distinctive regimes. For $d < 2$, we see that B decays in the form $B \sim 1/d^3$. This behavior is understood immediately, if we remember $f \sim 1/d^3$. For large $d > 2$, on the other hand, the interparticle interaction is relevant. We will explore this phase in the next subsection.

B. Scaling analyses

Here, we examine the data of f and B presented in Figs. 3 and 4 with use of some analytical predictions. First, we summarize recent remarkable predictions by Zaanen.¹ In his theory, B works as a mean field, which is to be determined self-consistently. The self-consistency equation to be solved is

$$f = C \frac{B}{\Sigma d^2} \left(\log \left(\frac{\Sigma d}{B} \right) + C' \right). \quad (13)$$

Appearance of logarithmic term is significant.¹ It is hard to solve this self-consistency equation. However, asymptotic form for $d \rightarrow \infty$ is calculated as follows:

$$f \sim e^{-C'' d^{2/3}}, \quad (14)$$

$$B \sim d^2 e^{-C'' d^{2/3}}. \quad (15)$$

In addition to Eq. (13), under the assumption that the string-meandering modes are irrelevant (frozen), he found another self-consistency condition,

$$f = C''' \frac{\sqrt{B}}{d^{3/2}}. \quad (16)$$

Note that the validity of this relation is checked, if we assume Eq. (11). Hence, this relation (13) may be realized for small d .

Besides those recent treatments, there exists an ingenious argument²⁵ in order to deal with entropic interaction. The argument, applied for quantum string (1), yields predictions different from the above. Below, we outline this argument: As is mentioned in the Introduction, in the path-integral picture, quantum string is identical to (classical) membrane. When quantum string is embedded in a free space, we can solve its mean deviation $\sim (\log l)^{1/2}$ with membrane’s linear

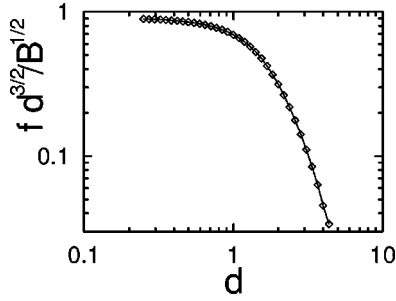


FIG. 5. $f d^{3/2}/B^{1/2}$ is plotted with use of the data shown in Figs. 3 and 4. This plot shows that the relation (16), which is valid for “compactified” string (Ref. 1), is realized for small d . On the other hand, for $d > 2$, it does not hold at all.

dimension l . Suppose that the wall width (mean membrane interval) is d , with use of this relation, one obtains an estimate of the surface S per one collision such as $d \sim (\log \sqrt{S})^{1/2}$. Assuming that each collision (contact-or-crossing) gives rise to entropy loss $\sim k_B \log 2$, we obtain the collision-induced energy gain per unit surface,

$$\sim k_B \log 2 e^{-C'' d^2}. \quad (17)$$

The argument is based on the assumption that the string would be disordered spatially as in the Einstein-like view of a crystal. In other words, short-wavelength fluctuations contribute to collisions. On the contrary, Ref. 1 emphasizes the significance of long-wavelength fluctuations. Our aim is to judge which picture is valid by means of first-principle simulations.

Guided by the above ideas, we will carry out scaling analyses. First, in Fig. 5, we plotted $f d^{3/2}/\sqrt{B}$ with use of the data shown in Figs. 3 and 4. Note that $f d^{3/2}/\sqrt{B}$ should be constant, if Eq. (16) holds. The scaling plot indicates that for $d < 2$, in fact, the scaled data are kept constant. On the contrary, for $d > 2$, the scaled data drop suddenly, suggesting that Eq. (16) does not hold any more. In consequence, we confirmed that for small d , string-meandering modes are irrelevant. These observations are consistent with those found in the previous subsection.

Secondly, let us turn to large- d regime. In Fig. 6, we plotted $f d^2/B$ against d/B with use of the data shown in Figs. 3 and 4. Note that the scale of abscissa is logarithmic.

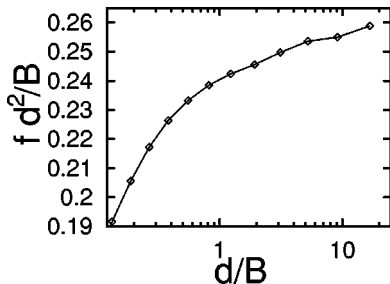


FIG. 6. $f d^2/B$ is plotted against d/B with use of the data shown in Figs. 3 and 4. For $d/B > 1$, the data approach a straight line asymptotically. This result indicates that the relation (13) is satisfied for the scaling region $d/B > 1$.

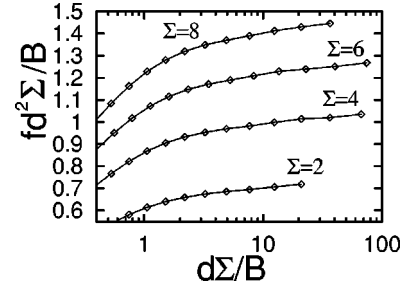


FIG. 7. Similar scaling analysis as Fig. 6 but for various $\Sigma = 2-8$. In the scaling regime $d\Sigma/B > 3$, slopes appear to be identical, suggesting that the constant C in Eq. (13) is universal with respect to arbitrary Σ .

Therefore, the data should align, if the relation (13) is satisfied. In fact, for scaling regime $d/B > 1$, we see that the scaled data get aligned, and exhibit a positive slope. This result justifies the validity of Eq. (13). Namely, the mean-field treatment of Ref. 1 appears to capture the essence of this physics. For exceedingly large d , eventually, numerical data become scattered (unstable) gradually. This is a symptom of numerical errors. Note that for exceedingly large d , the elasticity modulus B is very small (see Fig. 4) so that it suffers from tiny numerical errors. Hence, we cannot continue simulations for extremely large d .

In Fig. 7, we presented similar scaling data but for various $\Sigma = 2, 4, 6$ and 8 . The slopes of these data are identical. This fact tells that the constant C in Eq. (13) is indeed universal with respect to Σ . It is, however, suggested that C' is subjected to a correction to scaling, because plots do not overlap. We had found that scaling data for very small $\Sigma < 1$ are not described by Eq. (13). As a matter of fact, the slopes are almost vanishing. Breakdown of Eq. (13) for very small Σ is reasonable, because the equation is derived under continuum-limit treatment which is not justified for very small Σ . Therefore, such the region of small Σ lies out of the scope of Eq. (13).

C. Asymptotic form of f

In order to confirm the above observation, we investigate the asymptotic form of f for $d \rightarrow \infty$. As is mentioned in the previous subsection, f should obey the asymptotic form

$$f \sim e^{-C'' d^\alpha}, \quad (18)$$

with the exponent either $\alpha = 2/3$ (14) or $\alpha = 2$ (17). We expect that the former would be realized, because it is derived from Eq. (13), whose validity is checked in Sec. III B. We calculated α by means of the formula

$$\alpha = \frac{\log(\log f(d_1)/\log f(d_2))}{\log(d_1/d_2)}, \quad (19)$$

with respect to adjacent two data points of $d = d_1$ and d_2 depicted in Fig. 3. We plotted α in Fig. 8. The scale of abscissa $1/[(\log d_1 + \log d_2)/2]^2$ is chosen so as to achieve straight data alignment. We employed the least-square method in order to extrapolate the result for $d \rightarrow \infty$, and

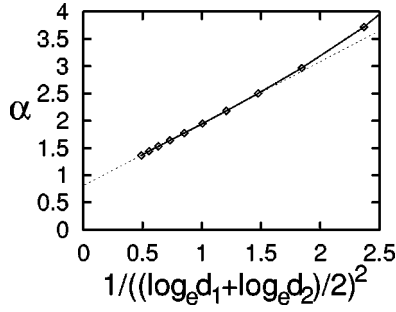


FIG. 8. Exponent α (19) is plotted with use of the data shown in Fig. 3. With the least-square method, we extrapolated the data so as to obtain $\alpha=0.808(1)$ for $d \rightarrow \infty$.

thereby, we obtained the estimate $\alpha=0.808(1)$. This result clearly supports $\alpha=2/3$ (14) rather than $\alpha=2$ (17). We notice that the convergence speed is rather slow; note that the abscissa scale of Fig. 8 is logarithmic. Hence, we found that the asymptotic form (14) is realized for extremely large d .

D. Mean fluctuation width Δ

So far, we have confirmed the validity of the relations (13) and (14). Underlying physics of these relations is astonishing;¹ namely, it is speculated that collisions rather contribute to straightening the quantum string. In this subsection, we will examine this remarkable scenario directly. We calculated the mean fluctuation deviation,

$$\Delta = \sqrt{\langle x_i^2 \rangle - \langle x_i \rangle^2}. \quad (20)$$

In Fig. 9, we plotted Δ for the same parameter conditions as in Fig. 3. To our surprise, Δ grows logarithmically ($\Delta \sim \log d$) for large d . That is, Δ is much less than the wall spacing d . This feature contradicts our intuition that the fluctuation might be proportional to the wall spacing d . Because Eq. (17) relies on this picture, it turned out that this picture does not hold for quantum string. Rather this result tells that

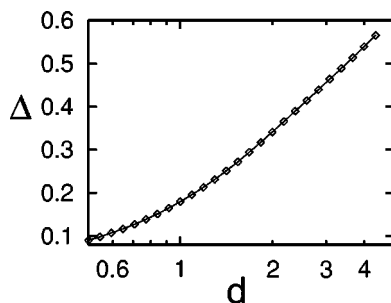


FIG. 9. Meandering-fluctuation width (20) is plotted for the same parameter range as that of Fig. 3. For $d > 2$, Δ grows logarithmically ($\Delta \sim \log d$). That is, the string's fluctuation is far less than the wall spacing d . This result indicates that the string is straightened by collisions.

string acquires stiffness with respect to short-wavelength fluctuations. That is, string's fluctuations are governed by long-wavelength modes.

IV. SUMMARY

We have investigated fluctuation-induced repelling interaction of quantum string described by the Hamiltonian (1). First, we have developed simulation scheme based on the idea of the density-matrix renormalization group.^{30–32} We found that the scheme works very efficiently. As is demonstrated in Fig. 1, ground-state energy is precise up to the eighth digit. Precision is crucial in our study, because we need to calculate second-order derivative in order to obtain the elasticity modulus B (12). Secondly, based on those preparations, we have performed extensive simulations. Simulation data suggest that two distinctive regimes exist: For small d , intraparticle interaction dominates so that simulation data are understood by ignoring line tension ($\Sigma=0$). That is, collision-induced energy cost f and the elasticity modulus B obey simple formulas such as $f, B \sim d^{-3}$. For large d , on the other hand, particles get correlated by line tension Σ , and physics becomes much harder to interpret. We made trials of several types of scalings in Figs. 5–7. From those scaling plots, in consequence, we found that the data of f and B agree with Zaanen's self-consistency condition (13). Moreover, we investigated the asymptotic form of f . We found $f \sim \exp(-C'd^\alpha)$ with $\alpha=0.808(1)$, which again supports Zaanen's result (14) rather than Eq. (17).

According to him, underlying physics of Eqs. (13) and (14) is quite peculiar; collisions with adjacent neighbors rather suppress short-range fluctuations, and consequently, quantum string is straightened macroscopically. In fact, we found that in Fig. 9, string's fluctuation deviation Δ is bounded within $\Delta \sim \log d$, which is far less than the wall spacing d . The above observations tell that in essence, quantum-string's ground state is governed by long-wavelength fluctuations. In this respect, it is decisively important to treat sufficiently long quantum string; otherwise we could not have observed those features mentioned above.

We have confirmed that owing to collisions, actually, order out of disorder sets in. This observation immediately leads an expectation that the stripe pattern observed in doped cuprates^{2–4} is stabilized by this mechanism. To verify this scenario definitely, one needs to explore “stacked” strings. As for stacked membranes, it has been known that N -membrane behavior is essentially the same as that of a single membrane confined between walls.^{17,21} That is, there is a relation, with which one obtains N -membrane behavior with respect to *single*-membrane result. It remains for future study to verify that similar relation holds as well as for stacked strings.

ACKNOWLEDGMENTS

Numerical calculation was performed on Alpha workstations of Theoretical Physics Group, Okayama University.

- ¹J. Zaanen, Phys. Rev. Lett. **84**, 753 (2000).
- ²J.M. Tranquada, B.J. Sternlieb, J.D. Axe, Y. Nakamura, and S. Uchida, Nature (London) **375**, 561 (1995).
- ³S. Wakimoto, G. Shirane, Y. Endoh, K. Hirota, S. Ueki, K. Yamada, R.J. Birgeneau, M.A. Kastner, Y.S. Lee, P.M. Gehring, and S.H. Lee, Phys. Rev. B **60**, R769 (1999).
- ⁴T. Noda, H. Eisaki, and S. Uchida, Science **286**, 265 (1999).
- ⁵J. Zaanen and O. Gunnarsson, Phys. Rev. B **40**, 7391 (1989).
- ⁶H.J. Schulz, Phys. Rev. Lett. **64**, 1445 (1990).
- ⁷M. Kato, K. Machida, H. Nakanishi, and M. Fujita, J. Phys. Soc. Jpn. **59**, 1047 (1990).
- ⁸D. Poilblanc and T.M. Rice, Phys. Rev. B **39**, 9749 (1989).
- ⁹M. Ichioka and K. Machida, J. Phys. Soc. Jpn. **68**, 4020 (1999).
- ¹⁰S.A. Kivelson, E. Fradkin, and V.J. Emery, Nature (London) **393**, 550 (1998).
- ¹¹C. Nayak and F. Wilczek, Phys. Rev. Lett. **78**, 2465 (1997).
- ¹²P. Prelovsek and X. Zotos, Phys. Rev. B **47**, 5984 (1993).
- ¹³S.R. White and D.J. Scalapino, Phys. Rev. Lett. **80**, 1272 (1998); **84**, 3021 (2000).
- ¹⁴C.S. Hellberg and E. Manousakis, Phys. Rev. Lett. **83**, 132 (1999); **84**, 3022 (2000).
- ¹⁵E. Fradkin, Phys. Rev. B **28**, 5338 (1983).
- ¹⁶W. Janke and H. Kleinert, Phys. Lett. A **117**, 353 (1986).
- ¹⁷W. Janke and H. Kleinert, Phys. Rev. Lett. **58**, 144 (1987).
- ¹⁸S. Leibler and A.C. Maggs, Phys. Rev. Lett. **63**, 406 (1989).
- ¹⁹R.R. Netz, Phys. Rev. E **51**, 2286 (1995).
- ²⁰N. Gouliarov and J.F. Nagle, Phys. Rev. E **58**, 881 (1998).
- ²¹H. Kleinert, Phys. Lett. A **257**, 269 (1999).
- ²²T. Yamamoto and Y. Kawashima, J. Phys. Soc. Jpn. **69**, 2715 (2000).
- ²³W. Helfrich, Z. Naturforsch. A **33a**, 305 (1978).
- ²⁴W. Helfrich and R.M. Servuss, Nuovo Cimento Soc. Ital. Fis., D **3D**, 137 (1984).
- ²⁵M.E. Fisher and D.S. Fisher, Phys. Rev. B **25**, 3192 (1982).
- ²⁶S.N. Coppersmith, D.S. Fisher, B.I. Halperin, P.A. Lee, and W.F. Brinkman, Phys. Rev. B **25**, 349 (1982).
- ²⁷J. Zaanen, M.L. Horbach, and W. van Saarloos, Phys. Rev. B **53**, 8671 (1996).
- ²⁸S.R. White, Phys. Rev. Lett. **69**, 2863 (1992).
- ²⁹S.R. White, Phys. Rev. B **48**, 10 345 (1993).
- ³⁰L.G. Caron and S. Moukouri, Phys. Rev. Lett. **76**, 4050 (1996).
- ³¹L.G. Caron and S. Moukouri, Phys. Rev. B **56**, R8471 (1997).
- ³²C. Zhang, E. Jeckelmann, and S.R. White, Phys. Rev. Lett. **80**, 2661 (1998).
- ³³Y. Nishiyama, Eur. Phys. J. B **12**, 547 (1999).